Rare Metal Materials and Engineering
Volume 54, Issue 10, October 2025
Available online at www.rmme.ac.cn

Science Press

Cite this article as: Chen Youhong, Lan Bo, Lin Yingying. Dynamic Recrystallization Behavior and Microstructure Evolution of As-extruded GH4710 Alloy Ingot[J]. Rare Metal Materials and Engineering, 2025, 54(10): 2483-2493. DOI: https://doi.org/10.12442/j.issn.1002-185X.20240555.

ARTICLE

Dynamic Recrystallization Behavior and Microstructure Evolution of As-extruded GH4710 Alloy Ingot

Chen Youhong, Lan Bo, Lin Yingying

AECC Beijing Institute of Aeronautical Materials, Beijing 100095, China

Abstract: A new triple melting method with hot extrusion process for GH4710 alloy ingots has been developed to overcome the difficulty in deformation of GH4710 alloy prepared by the casting and forging process. The as-extruded GH4710 alloy was analyzed through the isothermal compression experiment and metallographic analysis. The viscoelastic stress characteristics and dynamic recrystallization (DRX) behavior of the as-extruded GH4710 alloy were investigated during deformation at temperatures ranging from 1050 °C to 1120 °C and strain rates ranging from 0.01 s^{-1} to 5.00 s^{-1}. The true stress-true strain curves, average grain size, and DRX volume fraction were also obtained under various deformation conditions. Prediction models for DRX volume fraction and grain size of the as-extruded GH4710 alloy were established using the statistical regression method. The model was implanted into the Derform-3D software, and numerical simulation of the microstructure evolution of GH4710 alloy was conducted. Firstly, the isothermal compression simulations were conducted using the finite element method to verify the accuracy of prediction model. Subsequently, the prediction model was applied to perform an optimization analysis of the forging process for a turbine disk with a diameter of 300 mm. Results show a strong correlation between the simulated results and the actual microstructure of the turbine disk forged through the optimal process parameters. The optimal process parameters are deformation temperature of 1100 °C and forging speed of 0.2 mm/s. This established DRX prediction model can serve as a fundamental reference for understanding the microstructural evolution during the hot deformation process of as-extruded GH4710 alloy.

Key words: GH4710 alloy; triple melting; hot extrusion; dynamic recrystallization

1 Introduction

GH4710 alloy is a Ni-Cr-Co-based superalloy, which is used in the manufacturing of aero-engine turbine disks due to its excellent high-temperature strength, oxidation resistance, and sulfidation resistance. GH4710 alloy contains 6.5wt%–8.5wt% strengthening elements Al and Ti, forming 40vol%–45vol% γ' phase, which contributes to its ability to sustain the working temperature of 850 °C for long period and 980 °C for a certain period[1]. The high content of strengthening elements results in inferior forgeability of alloys during hot deformation, leading to cracks and inhomogeneous microstructure in the traditional process, such as duplexing melting, upsetting-drawing, and free forging, as shown in Fig. 1a, which thereby restrict the industrial applications.

A process involving triple melting, hot extrusion (HEX), and isothermal forging has been developed to address these issues, as illustrated in Fig. 1b. HEX has been identified as a key process to improve the forgeability of GH4710 alloy, as it provides a more intense triaxial compressive stress state for hard-to-deform alloys, compared with upsetting-drawing process, enabling the alloys to exhibit their maximum plasticity[2–4]. In Ref. [5–7], it was reported that HEX enhances the forgeability of GH4710 alloy and achieves surface integrity in bars. Furthermore, optimizing the microstructure to achieve the desired mechanical properties is important. Dynamic recrystallization (DRX) is a significant microstructural evolution mechanism that occurs during the hot deformation process, exerting a pronounced influence on both microstructure and macroscopic properties of the superalloy forgings. Therefore, DRX behavior of the as-extruded GH4710 alloy during the forging process requires further investigation.

Received date: October 28, 2024
Foundation item: Key Field Research Foundation of Beijing Institute of Aeronautical Materials (KJSC192309)
Corresponding author: Chen Youhong, Master, Senior Engineer, AECC Beijing Institute of Aeronautical Materials, Beijing 100095, P. R. China, Tel: 0086-10-62496699, E-mail: cyh198243@163.com

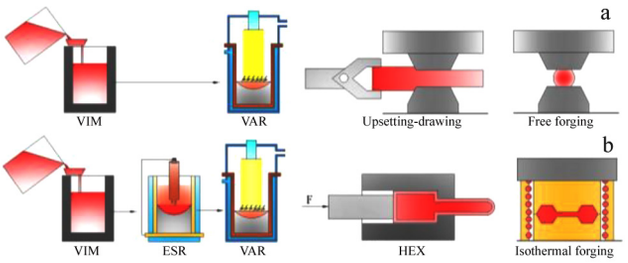

Fig.1 Traditional process (a) and developed process (b) for GH4710 alloy (VIM: vacuum induction melting; ESR: electroslag remelting; VAR: vacuum arc remelting)

DRX model has been developed for various materials, and the use of computational simulation to study the hot deformation performance of the alloy, especially its DRX behavior, is of high industrial application value. For instance, Cai[8] and Ji[9] et al formulated the models to predict the DRX volume fraction and grain size for the 33Cr23Ni8Mn3N heat-resistant steel. These models were integrated into the Deform-3D platform, where hot compression simulations were conducted using the finite element method (FEM). The congruence between the simulation outcomes and experiment data was notably high. Zhang et al[10] developed a cellular automaton model containing the effects of ellipsoidal δ phase particles on nucleation and grain boundary mobility, accurately describing the DRX behavior of Inconel 718 alloy. Yu et al[11] studied the DRX behavior of TC21 titanium alloy and established an evolution model to predict the grain size and DRX volume fraction. That model was verified through Deform-3D software and demonstrated a relative error within ±10%. Wan et al[12] established a DRX kinetics model for a TiAl-based alloy. The derived kinetics model was skillfully encoded into finite element codes, enabling a thorough investigation into the DRX behavior of the TiAl-based alloy during hot deformation processes. The correlation coefficient for the simulated values reached 0.956.

This research involved isothermal compression experiments to investigate the hot deformation behavior of the as-extruded GH4710 alloy. The influence of deformation conditions (temperature, strain rate $\dot{\varepsilon}$, and strain ε) on the microstructure was investigated using a metallographic microscope and an electron backscatter diffractometer (EBSD). DRX model was established for the as-extruded GH4710 alloy. Subsequently, the established model was implanted into Deform-3D software, and simulations of isothermal compression experiments and isothermal forging of turbine disk were conducted using FEM. A comparison between the simulation results and the experiment data was conducted to assess the model's applicability.

2 Experiment

The experimental material used in this research was GH4710 alloy, which is obtained through triple melting process, including VIM, ESR, and VAR. Table 1 provides the major chemical composition of GH4710 ingot specimens. The GH4710 ingot was processed into bars using canned HEX, which involves several steps: (1) encasing the GH4710 ingot within a 304 austenitic stainless-steel tube, known as a cladding layer; (2) extruding GH4710 bars; (3) modifying the as-extruded GH4710 bars into cylindrical specimens with 10 mm in diameter and 15 mm in length by wire cutter.

Table 1 Major chemical composition of GH4710 alloy (wt%)

Cr	Co	Al	Ti	W	Mo	B	Ni
17.70	15.96	2.70	4.91	1.51	3.30	0.02	Bal.

Fig.2 illustrates the experiment procedure. Cylindrical specimens underwent unidirectional isothermal compression experiments to achieve a strain of 60%. The isothermal compression experiments were conducted using the Gleeble-1500D thermal-mechanical simulator at strain rates of 0.01, 0.10, 1.00, and 5.00 s^{-1} and temperatures of 1050, 1080, 1100, and 1120 °C. Before the isothermal compression experiment, the cylindrical specimens were heated at heating rate of 10 °C·s^{-1} until the desired temperature was reached. After holding at desired temperature for 5 min, the isothermal compression experiment began. Once the targeted strain in height was achieved, water quenching was immediately conducted to preserve the microstructure for observation and analysis.

After compression, the deformed specimens were processed through several steps, such as cutting, grinding, polishing, and etching. The microstructures were examined using an optical microscope (OM, LEICA DMI5000 M) after the specimens were chemically etched with a solution composed of 100 mL CH_3CH_2OH, 100 mL HCl, and 50 g $CuCl_2$. EBSD specimens were electropolished with a solution of 10 mL H_2SO_4 and 40 mL CH_3OH at 20 V for 10 s. Then, the specimens were tested using a Zeiss field emission scanning electron microscope (SEM) equipped with an EBSD probe and analyzed with the Channel 5 software.

Afterwards, the Deform-3D software was used to integrate the DRX model and to perform simulations across various experimental conditions. These simulation results were compared against experiment data to validate the applicability of the DRX model for the as-extruded GH4710 alloy in both the compression experiment and the isothermal forging process of turbine disk. The isothermal forging of turbine disk

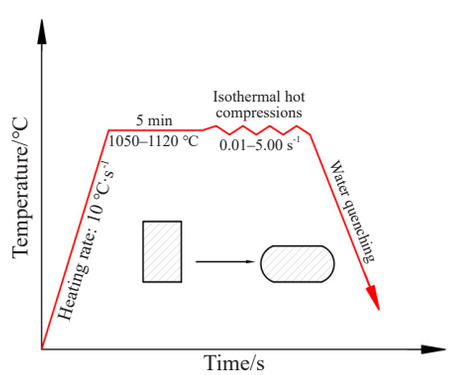

Fig.2 Experiment procedure

was conducted on the hydraulic press (2000 t). The detailed forging process of the turbine disk is illustrated in Fig.3.

3 Results and Discussion

3.1 Flow behavior analysis

Fig. 4 presents the true stress-true strain curves of as-extruded GH4710 alloy under various isothermal compression conditions, which demonstrate similarity with those of the as-forged GH4710 alloy[13]. A typical progression from rapid stress increase to a peak value can be observed, followed by a decline toward the steady state, with the increase in strain, indicating work hardening (WH), dynamic recovery (DRV), and DRX[14–16]. Initially, the compression experiment undergoes a WH phase. Before reaching the critical strain, DRX is not triggered, and WH is the dominant mechanism. As dislocations accumulate, WH is further intensified[17]. When the dislocation density surpasses the critical threshold, DRX is initiated, introducing a softening effect[18]. As strain escalates, DRX intensifies, and the softening effect becomes more pronounced, leading to a reduction in stress. Balancing the softening effect of DRX with WH results in a steady state stress[19].

Temperature and strain rate are pivotal for stress[20]. Increasing the temperature and decreasing the strain rate can substantially lower the stress[21–24]. Elevated temperatures promote the grain boundary migration and accelerate the vacancy diffusion, thereby enhancing DRX[25]. Consequently, the increased DRX leads to more significant softening effect and a subsequent decrease in stress. The reduction in strain rate at a constant deformation level leads to prolonged deformation duration, allowing for more sufficient growth of DRX grains. Furthermore, intensified DRX diminishes the impact of WH[26], causing flow stress to adjust in response to variations in temperature and strain rate.

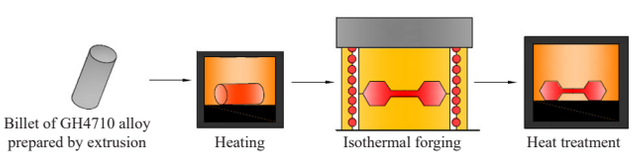

Fig.3 Forging process of turbine disk

3.2 Microstructure analysis

Fig.5 shows the microstructure evolution of the as-extruded GH710 alloy under strains of 10%, 30%, and 60% at temperature of 1100 °C and strain rate of 0.1 s^{-1}. As depicted in Fig. 5a, when the strain reaches 10%, the grains undergo elongation, and some grain boundaries form serrations, which serve as nucleation sites for DRX. At this stage, WH dominates, and the stress shows a tendency of sharp increase. After isothermal compression with strain of 30% (Fig. 5b), a DRX structure predominantly forms along the existing grain boundaries, displaying a distinctive necklace-type pattern. The softening effect of DRX becomes more apparent, resulting in the slowdown of the stress increase. The observed microstructure changes support the discontinuous dynamic recrystallization (DDRX) mechanism, particularly during hot working procedures[27–28]. Upon reaching the strain of 60% (Fig. 5c), DRX process is essentially complete, and the grain size simultaneously decreases. The softening effect of DRX and WH reaches a balance, and the stress is at stable state.

Fig. 6 presents EBSD analysis results of grain distributions in as-extruded GH4710 alloy specimens deformed to 60%, depicting the distribution of DRXed grains under different

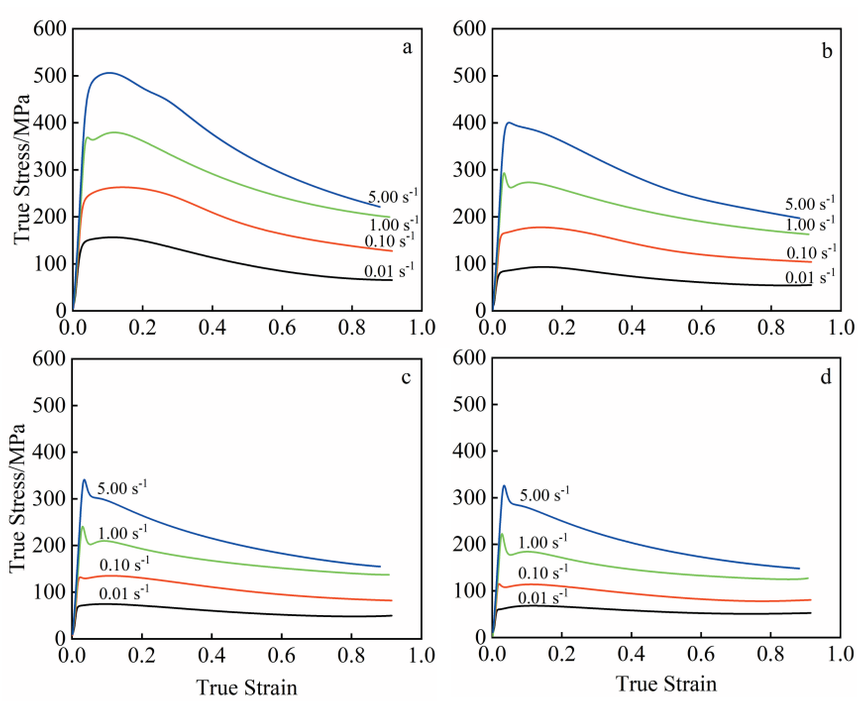

Fig.4 True stress-true strain curves of as-extruded GH4710 alloy at different temperatures: (a) 1050 °C, (b) 1080 °C, (c) 1100 °C, and (d) 1120 °C

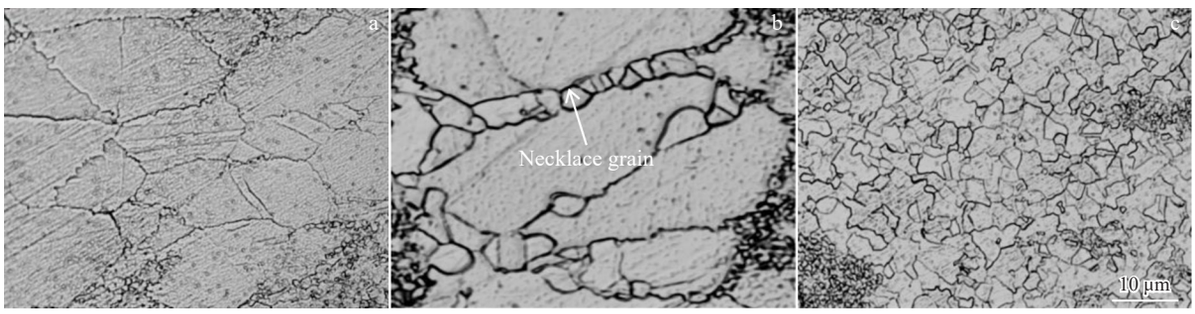

Fig.5 Microstructures of as-extruded GH4710 alloy specimens deformed to different strains at deformation conditions of 1100 °C and 0.1 s^{-1}: (a) ε=10%, (b) ε=30%, and (c) ε=60%

experiment conditions. At the strain rate of 0.1 s^{-1}, the original grains are transformed into deformed, substructured, and DRXed grains. Fig.6a illustrates that at 1050 °C, DRXed, substructured, and deformed grains account for 59.2%, 32.8%, and 8.0%, respectively. When the temperature increases from 1050 °C to 1120 °C, the proportion of DRXed and substructured grains increases continuously to 62.4% and 37.6%, respectively, and the proportion of deformed grains decreases from 8.0% to 0.0%, indicating that the deformed grains are continuously transformed into substructured and DRXed grains with the increase in temperature (Fig.6b–6d). Notably, at the temperature of 1100 °C (Fig.6c), the deformed grains are completely transformed into equiaxed DRXed grains and substructured grains. Comparing Fig. 6d with 6f, at the constant temperature of 1120 °C and different strain rates of 0.10, 1.00, and 5.00 s^{-1}, the area of the blue region is significantly larger with the increase in strain rate. When the strain rate increases from 0.10 s^{-1} to 1.00 s^{-1}, the percentage of DRXed grains increases from 62.4% to 93.2%, indicating a significant increase in DRX content. The increase in strain rate provides enough activation energy for the nucleation of DRXed grains, so the percentage of DRXed grains and the nucleation rate are increasing[29–30]. In addition, a small number of DRXed grains existing within the substructured grains indicate that continuous dynamic recrystallization (CDRX) also occurs[31–32], but it is not the dominant mechanism.

Fig. 7 illustrates the inverse pole figures (IPFs) of as-extruded GH4710 alloy specimens deformed to 60% under different experiment conditions. When the temperature is 1050 °C and the strain rate is 0.1 s^{-1} (Fig. 7a), the original grains and DRXed grains are elongated along the direction perpendicular to the compression axis. When the temperature increases to 1080 °C (Fig. 7b), DRXed grains evolve into equiaxed grains. As the temperature further increases to 1120 °C, the size of DRXed grains increases to 3.6 μm (Fig. 7d). This increase results from the higher temperature, which provides sufficient energy for DRX grain growth.

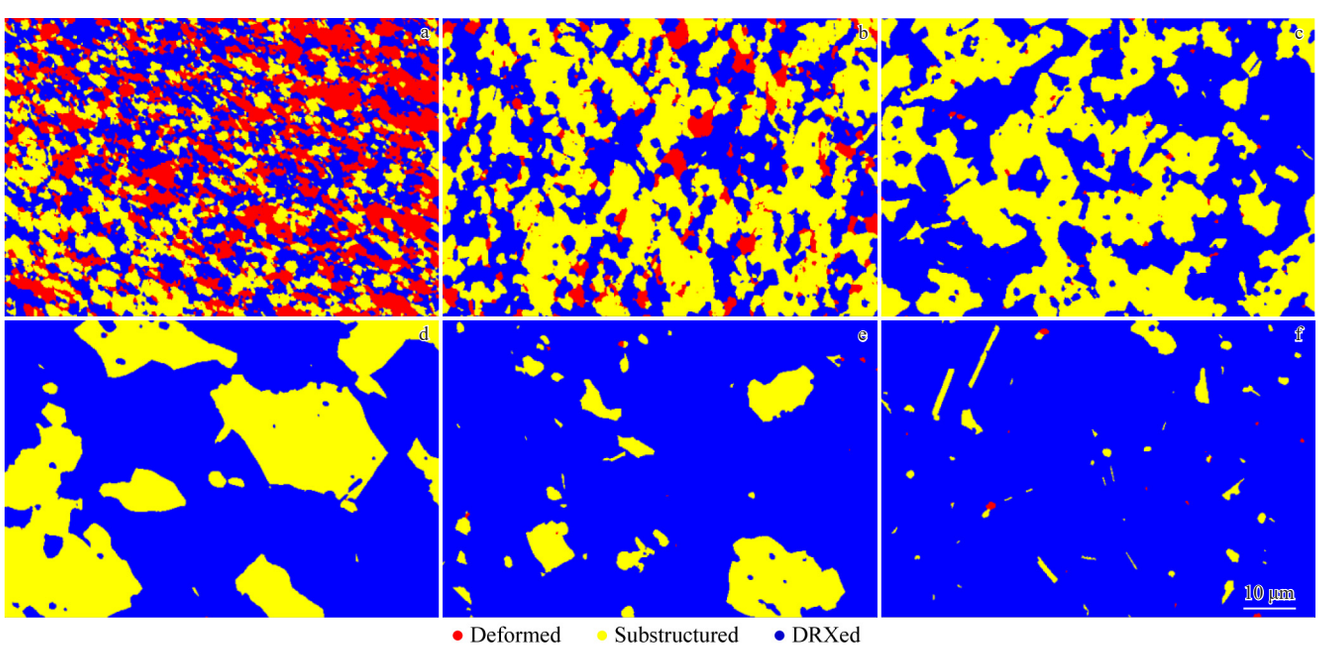

Fig.6 EBSD analysis results of grain distributions in as-extruded GH4710 alloy specimens deformed to 60% under different conditions: (a) 1050 °C/0.10 s^{-1}; (b) 1080 °C/0.10 s^{-1}; (c) 1100 °C/0.10 s^{-1}; (d) 1120 °C/0.10 s^{-1}; (e) 1120 °C/1.00 s^{-1}; (f) 1120 °C/5.00 s^{-1}

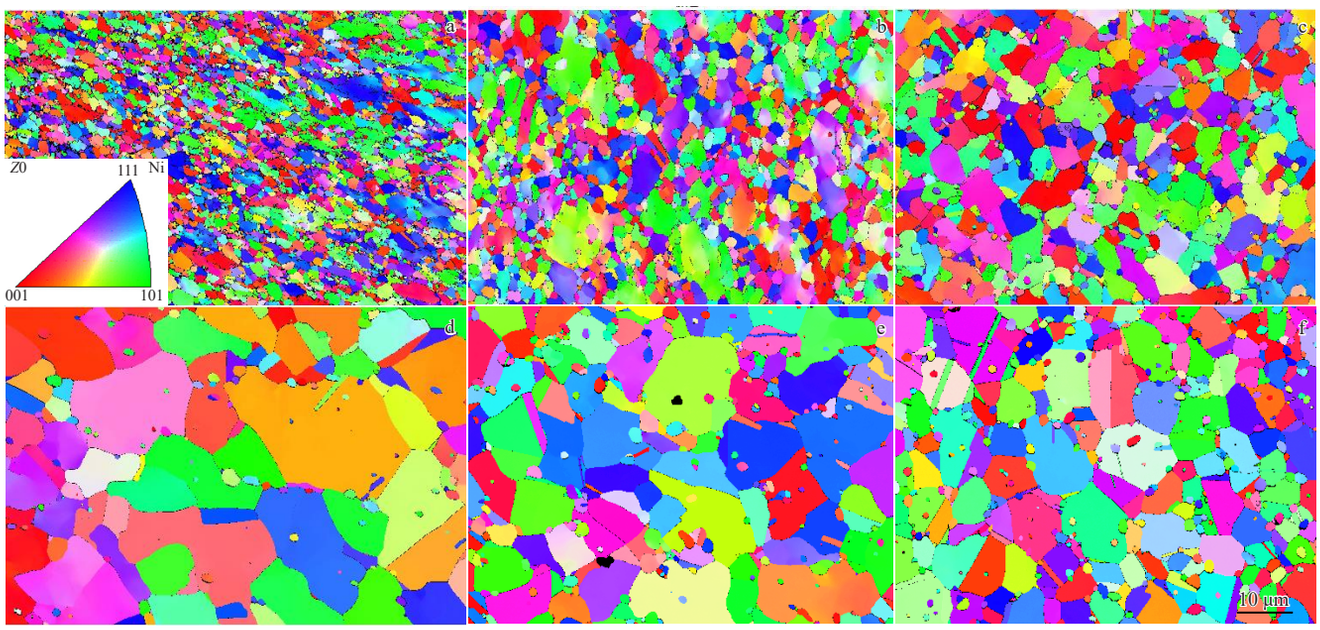

Fig.7 IPFs of as-extruded GH4710 alloy specimens deformed to 60% under different conditions: (a) 1050 °C/1.00 s^{-1}; (b) 1080 °C/1.00 s^{-1}; (c) 1100 °C/1.00 s^{-1}; (d) 1120 °C/1.00 s^{-1}; (e) 1100 °C/0.10 s^{-1}; (f) 1120 °C/0.10 s^{-1}

Comparing Fig. 7d with 7f, at 1120 °C, DRXed grains are decreased in size with the increase in strain rate from 0.10 s^{-1} to 1.00 s^{-1}, due to the shortened deformation duration, which prevents the adequate growth of DRX grains.

3.3 Model establishment for DRX volume fraction and DRX average grain size

During hot deformation, DRX occurs when the critical strain is reached, and DRX degree can be expressed by the DRX volume fraction, which can be estimated by the extrapolation method through flow stress data from Fig. 8a. DRX volume fraction X_{DRX} can be expressed as Eq. (1)[33], as follows:

$$X_{DRX} = (\sigma_{drvss} - \sigma_{drxx})/(\sigma_{drvss} - \sigma_{drxss}) \quad \varepsilon \geqslant \varepsilon_c \tag{1}$$

where σ_{drxx} denotes DRX instantaneous flow stress; σ_{drvss} and σ_{drxss} refer to the steady-state stresses of DRV and DRX, respectively; ε is strain; ε_c is critical strain.

σ_{drxx} can be directly derived from the stress-strain (σ - ε) curve. σ_{drvss} and σ_{drxss} in Fig. 8b can be determined according to Ref.[34]. A line is drawn along the tangent at the critical strain ε_c on the θ-σ curve. The line is extended to intersect with the line θ=0. The corresponding stress of the intersection is σ_{drvss}. When the curve once again intersects the line θ =0, the corresponding stress is σ_{drxss}. The positions of σ_{drvss} and σ_{drxss} are on the σ-ε curve, as shown in Fig.8a.

DRX volume fractions under different conditions are obtained by Eq. (1), and the results are drawn by Origin software, as shown in Fig.9.

The determination of DRX volume fraction is simplified by the DRX kinetic equation, which is modeled using the JMAK equation[35–36]:

$$X_{DRX} = 1 - \exp\left[-\beta_d\left(\frac{\varepsilon - \varepsilon_c}{\varepsilon_{0.5}}\right)\right]^{k_d} \quad \varepsilon \geqslant \varepsilon_c \tag{2}$$

$$\varepsilon_{0.5} = a_2 d_0^{n_2} \dot{\varepsilon}^{m_2} \exp(Q_2/RT) \tag{3}$$

where $\varepsilon_{0.5}$ indicates the strain corresponding to 50% DRX volume fraction; β_d and k_d denote the Avrami material

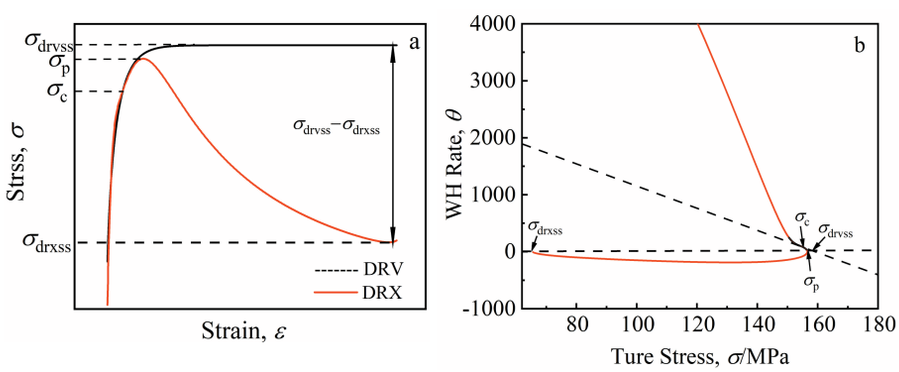

Fig.8 DRX and DRV curves (a); extrapolation method to obtain σ_{drvss} and σ_{drxss} (b)

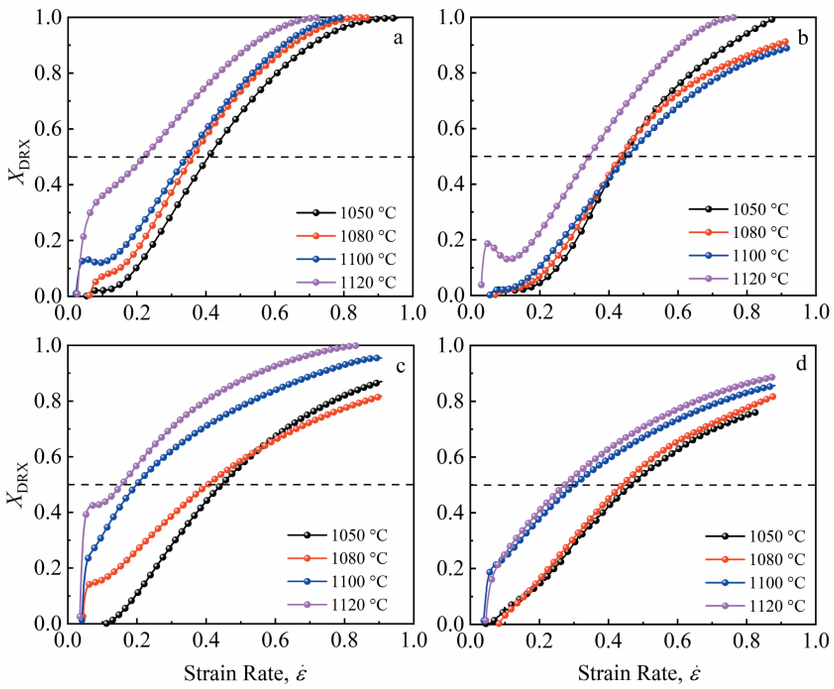

Fig.9 DRX volume fractions of as-extruded GH4710 alloy deformed under different strain rates: (a) 0.01 s^{-1}, (b) 0.10 s^{-1}, (c) 1.00 s^{-1}, and (d) 5.00 s^{-1}

constants; a_2, n_2, and m_2 represent the material constants; Q_2 denotes the DRX activation energy; d_0 denotes the initial grain size; R is gas constant; T is temperature.

Take logarithm of Eq. (2), and Eq. (4) can be obtained as follows:

$$\ln\left[-\ln\left(1-X_{DRX}\right)\right]=\ln\beta_d+k_d\ln\left[\left(\varepsilon-\varepsilon_c\right)/\varepsilon_{0.5}\right] \quad (4)$$

The strains at X_{DRX}=50% under different conditions are listed in Table 2. Combined with the calculated DRX volume fraction and critical strain, the linear relationship between $\ln[-\ln(1-X_{DRX})]$ and $\ln[(\varepsilon-\varepsilon_c)/\varepsilon_{0.5}]$ under different conditions can be determined, as shown in Fig.10.

k_d is the slope of the fitted line, and $\ln\beta_d$ is the intercept of the fitted line. A linear fit is performed on all data, and the parameters of the fitting line are k_d=1.541 and β_d=1.035.

Take logarithm of Eq. (3), and Eq. (5) is calculated as follows:

$$\ln\varepsilon_{0.5}=\ln a_2+n_2\ln d_0+m_2\ln\dot{\varepsilon}+Q_2/RT \quad (5)$$

The influence of grain size is not considered for the moment, so n_2=0. Thus, Eq.(5) can be expressed as follows:

$$\ln\varepsilon_{0.5}=\ln a_2+m_2\ln\dot{\varepsilon}+Q_2/RT \quad (6)$$

Table 2 $\varepsilon_{0.5}$ results under different conditions

Strain rate/s^{-1}	Temperature/°C			
	1050	1080	1100	1120
0.01	0.408	0.362	0.344	0.223
0.10	0.440	0.435	0.455	0.344
1.00	0.446	0.405	0.199	0.158
5.00	0.516	0.440	0.301	0.274

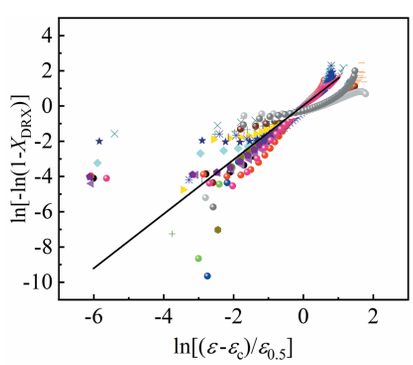

Fig.10 Relationship between $\ln[-\ln(1-X_{DRX})]$ and $\ln[(\varepsilon-\varepsilon_c)/\varepsilon_{0.5}]$ under different conditions

At a certain temperature or a certain strain rate, Eq. (7) or Eq.(8) can be obtained, respectively:

$$m_2=\left.\frac{\partial\ln\varepsilon_{0.5}}{\partial\ln\dot{\varepsilon}}\right|_T \quad (7)$$

$$Q_2=\left.\frac{\partial\ln\varepsilon_{0.5}}{\partial(1/T)}\right|_{\varepsilon} \quad (8)$$

The relationships of $\ln\varepsilon_{0.5}$-$\ln\varepsilon$ and $\ln\varepsilon_{0.5}$-$1/T$ are shown in Fig. 11. After linear fitting, m_2 value at different deformation temperatures and Q_2 value at different strain rates can be obtained. The average values of m_2 and Q_2 are 0.0296 and 14 236.64, respectively. The calculated a_2 value is 0.341.

Hence, the model of DRX volume fraction can be obtained as follows:

$$X_{DRX}=1-\exp\left[-1.035\left(\frac{\varepsilon-\varepsilon_c}{\varepsilon_{0.5}}\right)\right]^{1.541} \quad \varepsilon\geqslant\varepsilon_c \quad (9)$$

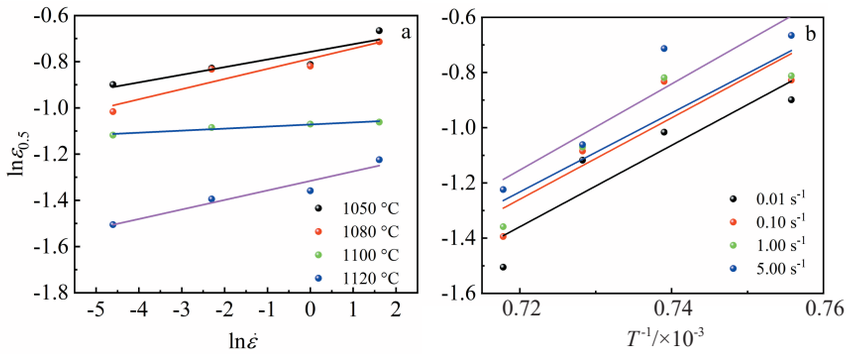

Fig.11 Relationships of $\ln\varepsilon_{0.5}$-$\ln\dot{\varepsilon}$ (a) and $\ln\varepsilon_{0.5}$-$1/T$ (b)

$$\varepsilon_{0.5} = 0.341\dot{\varepsilon}^{0.029}\exp(14236.64/RT) \quad (10)$$

The comparison results between the calculated and experimental results of X_{DRX} and average grain size during the isothermal compression under conditions of 1100 °C and 0.1 s^{-1} are shown in Fig. 12. It can be seen that the calculated results agree well with the experiment results.

For DRX, a certain functional relationship exists between DRX average grain size (d_{DRX}) and the Z parameter, as shown in Eq.(11):

$$d_{DRX} = CZ^a \quad (11)$$

where C and a are material parameters.

Take logarithm of Eq. (11), and Eq. (12) is obtained as follows:

$$\ln d_{DRX} = \ln C + a\ln Z \quad (12)$$

Table 3 shows DRX average grain size under different conditions. According to Eq. (12), the linear regression in Fig.13 is determined to obtain the material parameters ln$C$ and a, as shown in Table 4. The ln$C$ value is the intercept of the fitting line, and a value is the slope of the fitting line. The average values of a and C are −0.079 and 352.1, respectively. Substituting ln$C$ and a into Eq. (12), the model of DRX average grain size of the as-extruded GH4710 alloy can be obtained, as follows:

$$d_{DRX} = 0.352\times10^3 Z^{-0.079} \quad (13)$$

3.4 Application and validation of established models based on Deform-3D

FEM can effectively reduce the drawbacks of the traditional trial and error method, and it is highly efficient in current research on material processing. The established DRX model provides support for studying the hot deformation process of as-extruded GH4710 alloy. To verify the model feasibility, it was implemented into Deform-3D software for experiment simulation. The simulation of the specimens was conducted under the following boundary conditions: the convective heat transfer coefficient between the specimen and the air is 0.02 N·(s·mm·°C)$^{-1}$; the heat transfer coefficient between the

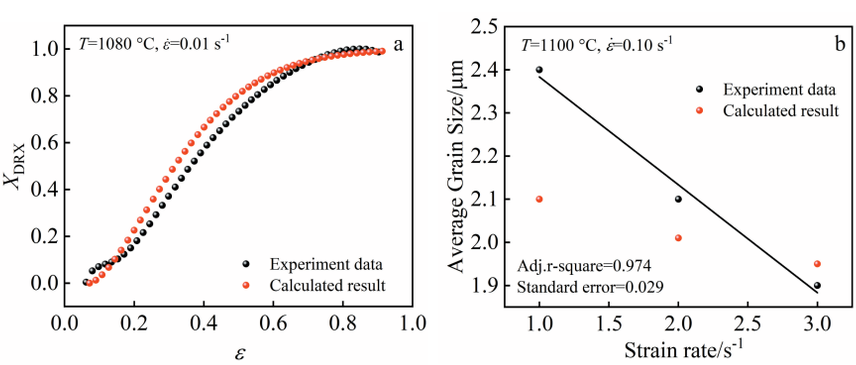

Fig.12 Comparison results of calculated and experiment results of X_{DRX} (a) and average grain size (b)

Table 3 Results of average grain size and parameter Z of as-extruded GH710 alloy under different conditions

Strain rate/s^{-1}	Temperature/°C							
	1050		1080		1100		1200	
	ln$Z$	lnd_{DRX}	ln$Z$	lnd_{DRX}	ln$Z$	lnd_{DRX}	ln$Z$	lnd_{DRX}
0.01	30.549	1.098	29.770	29.269	29.269	-	28.783	29.269
0.10	32.852	0.641	32.072	31.572	31.572	1.589	31.085	31.572
1.00	35.154	0.095	34.375	33.874	33.874	1.589	33.388	33.874
5.00	36.764	0.262	35.984	35.484	35.484	1.435	34.997	35.484

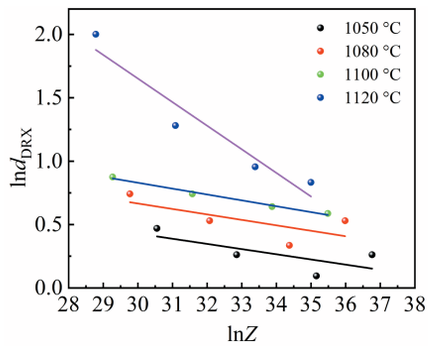

Fig.13 Relationship between $\ln d_{DRX}$ and $\ln Z$ under different conditions

Table 4 Materials constants *a* and *C* of as-extruded GH710 alloy under different conditions

Temperature/℃	1050	1080	1100	1120
a	−0.041	−0.043	−0.046	−0.186
ln*C*	1.655	1.957	2.22	7.235
Average value of *a*		−0.079		
Average value of ln*C*		352.1		

specimen and the mold is 11 N·(s·mm·℃)$^{-1}$; the coefficient of friction between the specimen and the mold is 0.3; the initial grain size is 12.5 μm. The average grain size is obtained after simulation and compared with the experiment data.

Fig. 14 shows the average grain size distribution under conditions of 1000 °C and 0.1 s^{-1}. The average grain size distribution is mainly divided into three zones. Zone I is the core area with large deformation, which has a small grain size; zone II is the difficult-to-deform zone, which is characterized by large grain sizes; zone III is the free deformation zone, where the deformation is less than that in zone I but more than that in zone II with intermediate grain sizes, compared with those of zone I and zone II. This phenomenon is in accordance with the fundamental principles of the upsetting process. The

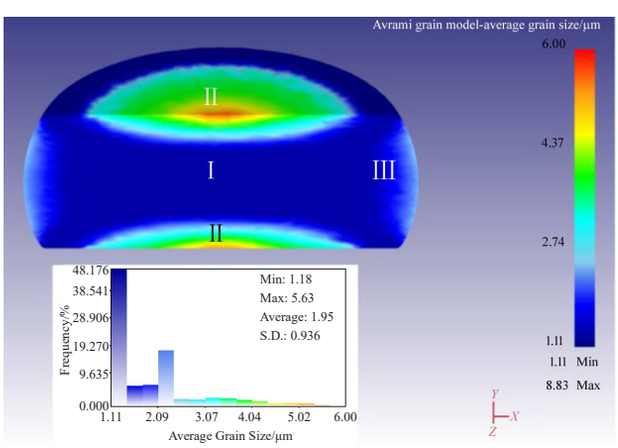

Fig.14 Average grain size distribution of as-extruded GH4710 alloy deformed under conditions of 1000 °C and 0.10 s^{-1} after upsetting

average grain size at 1100 °C obtained by simulation is shown in Table 5, which is highly consistent with the experimental results. This characteristic confirms that the established DRX model can be used to predict the hot deformation of the as-extruded GH4710 alloy.

To further validate the accuracy of DRX model for the as-extruded GH4710 alloy, a simulation of the isothermal forging for the turbine disk with a diameter of 300 mm was conducted. Fig.15 shows the finite element model of a turbine disk, which is simulated from a cylindrical billet of 150 mm in diameter and 300 mm in length. To simulate the isothermal forging of a turbine disk, three distinct sets of deformation conditions were selected: the temperatures are 1050, 1100, and 1120 ℃, and the die velocities are 0.1, 0.2, and 0.5 mm/s.

Fig. 16 illustrates DRX volume fraction and average grain size throughout the isothermal forging of the turbine disk. The DRX volume fraction and average grain size distribution in the turbine disk are uniform. Lower DRX volume fraction (Fig. 16a) and smaller average grain size (Fig. 16b) can be observed in the top and bottom bosses due to smaller deformation. Fig. 16c presents the statistical analysis of the DRX volume fraction and average grain size under different conditions, separately. It can be observed that at low die velocity (0.1 – 0.2 mm·s^{-1}), the higher the temperature, the higher the DRX volume fraction, but it starts to decrease after

Table 5 Simulated and measured average grain size of as-extruded GH4710 alloy deformed at 1100 ℃ and different strain rates

Strain rate/s^{-1}	Simulated average grain size/μm	Measured average grain size/μm
0.01	2.09	2.1
0.10	1.99	1.7
1.00	1.92	1.4

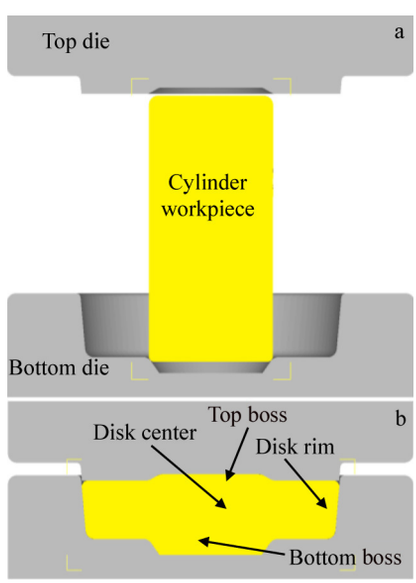

Fig.15 Finite element model of isothermal forging of as-extruded GH4710 alloy turbine disk: (a) initial state; (b) final state

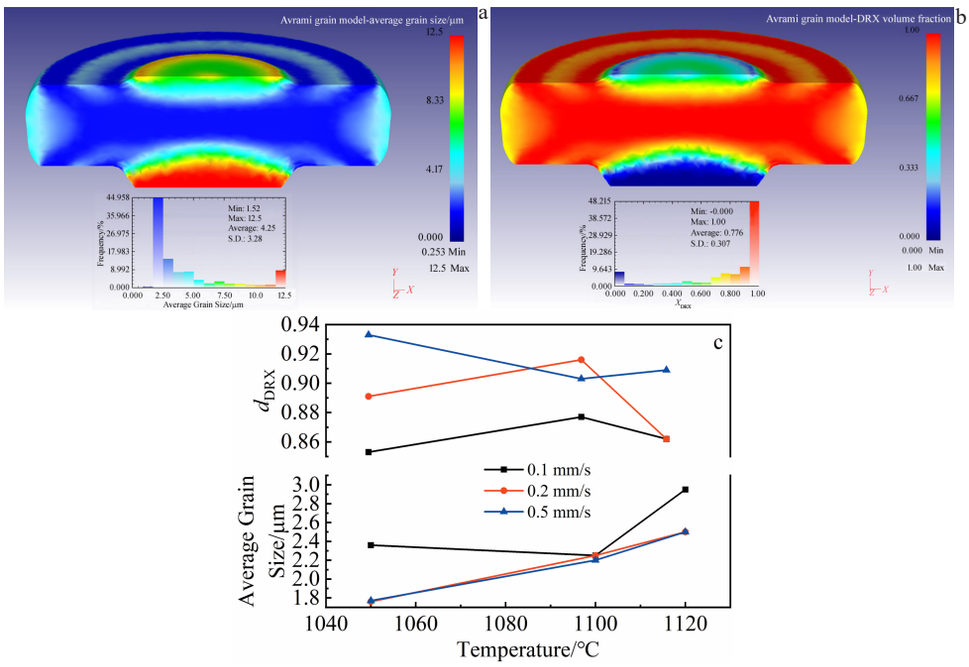

Fig.16 Simulation results of turbine disk under different conditions after isothermal forging: (a) average grain size; (b) DRX volume fraction; (c) variation trend of average grain size and DRX volume fraction

reaching 1100 °C. However, at high die velocity (0.5 mm·s^{-1}), the DRX volume fraction exhibits an overall decreasing trend with the increase in temperature. The average grain size demonstrates a general growth trend with the increase in temperature. The optimal DRX volume fraction and average grain size can be achieved at the temperature of 1100 °C and die velocity of 0.1 – 0.2 mm·s^{-1}. According to the simulation results, the condition of 1100 °C and 0.2 mm·s^{-1} was chosen for experimental verification.

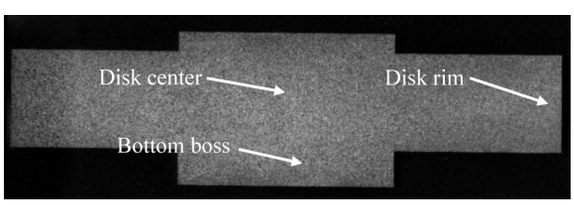

Fig.17 Schematic diagram of longitudinal analysis area of turbine disk

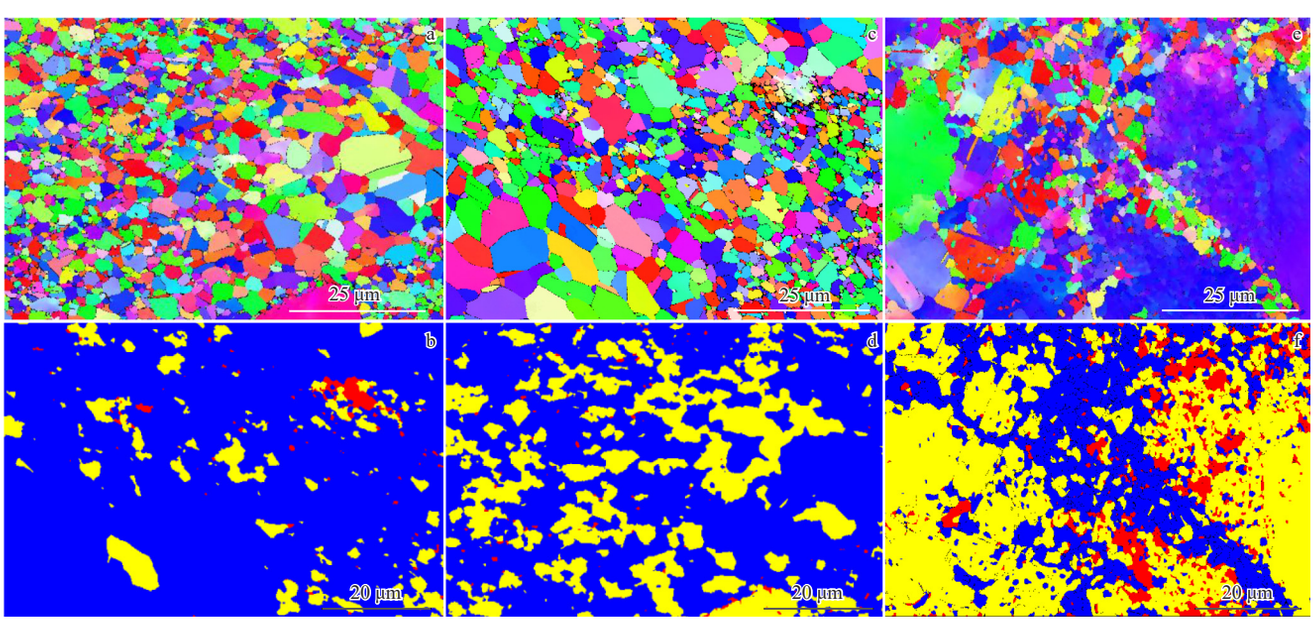

Fig.18 EBSD analysis results of average grain size and DRX volume fraction of turbine disk deformed at 1100 °C and 0.2 mm/s after isothermal forging: (a–b) disk center; (c–d) disk rim; (e–f) bottom boss

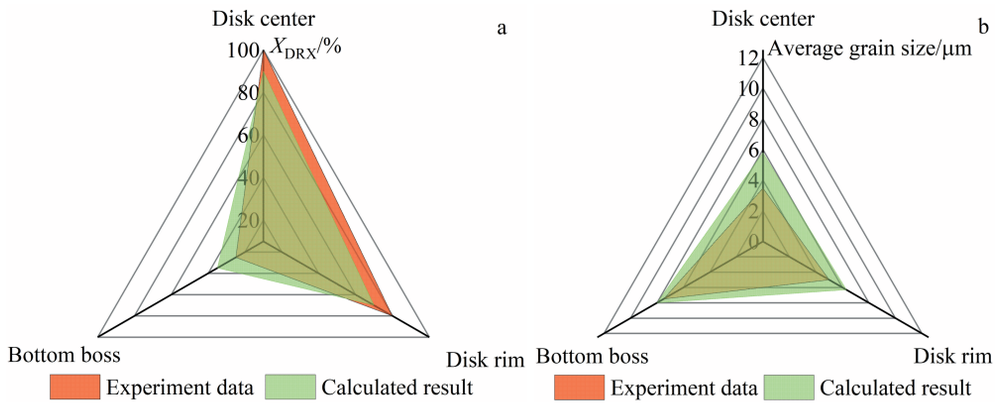

Fig.19 Comparison of experiment and calculated results of DRX volume fraction (a) and average grain size (b) of different areas on turbine disk deformed at 1100 °C and 0.2 mm/s

Fig. 17 illustrates the analysis area of turbine disk, and Fig. 18 shows EBSD analysis of the average grain size and DRX volume fraction of the turbine disk. Multiple specimens were extracted from the turbine disk to observe both the grain size and DRX volume fraction. The disk center has DRX volume fraction of 90%, accompanied by an average grain size of 5.8 mm. In the disk rim area, the DRX volume fraction is 70% with an average grain size of 6.3 μm. The bottom boss has an approximate DRX volume fraction of 35%, accompanied by an average grain size of 8.0 μm. Fig. 19 presents the comparison results of the calculated and experiment results of DRX volume fraction and average grain size at various positions on the turbine disk. The comparison shows a high degree of consistency. It can be seen that this model can accurately predict the DRX behavior of the as-extruded GH4710 alloy during the hot deformation process.

4 Conclusions

1) Both temperature and strain rate significantly influence the DRX behavior of the as-extruded GH4710 alloy. The occurrence of DRX behavior becomes more pronounced with the increase in temperature and strain rate. Additionally, the size of DRXed grains is increased with the increase in temperature and the decrease in strain rate. The primary mechanism for DRX nucleation is DDRX, complemented by CDRX process.

2) Based on the stress-strain curves and microstructure characteristics, the model for the prediction of DRX volume fraction is as follows: $X_{DRX}=1-\exp\left\{-1.035\left[(\varepsilon-\varepsilon_c)/\varepsilon_{0.5}\right]\right\}^{1.541}$ ($\varepsilon\geqslant\varepsilon_c$) with $\varepsilon_{0.5}=0.341\dot{\varepsilon}^{0.029}\exp(14236.64/RT)$. The prediction model of average grain size is $d_{DRX}=0.352\times10^3Z^{-0.079}$.

3) The simulation results are highly consistent with the experiment data, confirming the reliability of these prediction models as tools for predicting the behavior of the as-extruded GH4710 alloy during hot deformation process.

References

1 Jia Weiping, Bin Miao, Meng Huawu. *Advanced Materials Research*[J], 2012, 538: 1322

2 Wen Hongning, Jin Junsong, Teng Qing *et al*. *The Chinese Journal of Nonferrous Metals*[J], 2022, 32(9): 2664 (in Chinese)

3 Shi Yingnan, Sun Shaobin, Qu Jinglong *et al*. *Powder Metallurgy Industry*[J], 2024, 34(1): 124 (in Chinese)

4 Li Huizhong, Yang Lei, Wang Yan *et al*. *Journal of Materials Engineering*[J], 2020, 48(9): 115

5 Chen Youhong, Wang Shuyun, Han Bo. *Hot Working Technology*[J], 2015, 44(12): 1 (in Chinese)

6 Chen Youhong, Lan Bo, Sun Xing *et al*. *Transctions of Materials and Heat Treatment*[J], 2020, 41(8): 42 (in Chinese)

7 Chen Youhong, Lan Bo, Sun Xing *et al*. *Rare Metal Materials and Engineering*[J], 2024, 53(9): 2555 (in Chinese)

8 Cai Zhongman, Ji Hongchao, Pei Weichi *et al*. *Materials*[J], 2020, 13(6): 1282

9 Ji Hongchao, Cai Zhongman, Pei Weichi *et al*. *Journal of Materials Research and Technology*[J], 2020, 9(3): 4340

10 Zhang Fuxiang, Liu Dong, Yang Yanhui *et al*. *Modelling and Simulation in Materials Science and Engineering*[J], 2019, 27(3): 035002

11 Yu Xinping, Dong Hongbo. *Journal of Plasticity Engineering*[J], 2015, 22(1): 39

12 Wan Zhipeng, Sun Yu, Hu Lianxi *et al*. *Materials & Design*[J], 2017, 122: 11

13 Yu Qiuying, Zhang Maicang, Dong Jianxin *et al*. *Materials for Mechanical Engineering*[J], 2012, 36(12): 62

14 Li Yang, Li Min, Zhao Guanghui *et al*. *Materials Research Express*[J], 2024, 11(3): 036524

15 Jia Zhi, Gao Zexi, Ji Jinjin *et al*. *Rare Metals*[J], 2021, 40(8): 2083

16 Xie Bingchao, Zhang Baoyun, Ning Yongquan *et al*. *Journal of Alloys and Compounds*[J], 2019, 786: 636

17 Li Huizhong, Yang Lei, Wang Yan *et al*. *Materials Characterization*[J], 2020, 163: 110285

18 Wan Zhipeng, Hu Lianxi, Sun Yu *et al*. *Vacuum*[J], 2018, 155: 585

19 Niu Yanxia, Hou Jian, Ning Fangkun *et al*. *Journal of Rare Earths*[J], 2020, 38:665
20 Li Zhou, Chen Yunbo, Wei Shizhong *et al*. *Journal of Alloys and Compounds*[J], 2019, 802: 118
21 Arab Ali, Guo Yansong, Sktani Zhwan Dilshad Ibrahim *et al*. *Intermetallics*[J], 2022, 147: 107601
22 Zhang Rui, Wang Dongjun, Huang Lujun *et al*. *Journal of Alloys and Compounds*[J], 2017, 722: 970
23 Gu B, Chekhonin P, Xin S W *et al*. *Journal of Alloys and Compounds*[J], 2021, 876: 159938
24 Sun J Z, Li M Q, Li H. *Journal of Alloys and Compounds*[J], 2018, 730: 533
25 Ren Facai, Chen Fei, Chen Jun *et al*. *Journal of Manufacturing Process*[J], 2018, 31: 640
26 Kumar S S S, Raghu T, Bhattacharjee P P *et al*. *Journal of Alloys and Compounds*[J], 2017, 709: 394
27 Xie Bingchao, Yu Hao, Sheng Tao *et al*. *Journal of Alloys and Compounds*[J], 2019, 803: 16
28 Zhao Jiuhui, Deng Yunlai, Tang Jianguo. *Journal of Materials Research and Technology*[J], 2020, 9(4): 8001
29 Ding Ning, Du Wenbo, Li Shubo *et al*. *Journal of Magnesium and Alloys*[J], 2023, 13(1): 161
30 Zhang Yuqing, Quan Guozheng, Lei Sheng *et al*. *Materials*[J], 2022, 15(16): 5593
31 Huang K, Logé R E. *Materials & Design*[J], 2016, 111: 548
32 Tian Yuxing, Liu Cheng, Cao Hailong *et al*. *Rare Metal Materials and Engineering*[J], 2019, 48(11): 3764 (in Chinese)
33 Zhang Cunsheng, Wang Cuixue, Guo Ran *et al*. *Journal of Alloys and Compounds*[J], 2019, 773: 59
34 Lin Y C, Chen X M, Wen D *et al*. *Computational*[J], 2014, 83: 282
35 Nam A, Turdimatov M, Kawalla R *et al*. *Steel Research International*[J], 2019, 90(6): 1800309
36 Zyguła K, Cichocki K, Kowalczyk K *et al*. *JOM*[J], 2024: 76(9): 5193

GH4710合金铸锭挤压后的动态再结晶行为及微观结构演变

陈由红，兰　博，林莺莺
(中国航发北京航空材料研究院，北京 100095)

摘　要：研发了一种三联冶炼GH4710合金铸锭热挤压新工艺，以克服GH4710合金采用铸锻工艺变形难的问题。对挤压态GH4710合金进行了等温压缩实验和金相研究，分析了该合金在变形温度为1050～1120 ℃、应变速率为0.01～5.00 s^{-1}条件下的流变应力特征、动态再结晶（DRX）行为及微观组织演变。在不同的变形条件下，获得了真应力-真应变曲线、平均晶粒尺寸以及动态再结晶体积分数。采用统计回归方法，建立了挤压态GH4710合金的DRX体积分数和晶粒尺寸的预测模型。将模型写入Derform-3D软件中，并对该合金微观组织演化进行数值模拟。首先，通过有限元方法对等温压缩进行数值模拟，证实了模型的准确性。再者，将模型应用于直径为300 mm的涡轮盘进行锻造工艺优化分析。结果表明：模拟所得的结果与采用最优工艺参数锻造的涡轮盘的实际微观结构之间存在很强的相关性。最优工艺参数为变形温度1100 ℃、锻造速度0.2 mm/s。这一DRX预测模型可作为GH4710合金铸锭挤压后热变形过程微观结构演变的基准参考。

关键词：GH4710合金；三联冶炼；热挤压；动态再结晶

作者简介：陈由红，男，1981年生，硕士，高级工程师，中国航发北京航空材料研究院，北京 100095，电话：010-62496699，E-mail：cyh198243@163.com